Mechanics of Advanced Composite Structures 5 (2018) 67-74

Semnan University

Mechanics of Advanced Composite Structures

Journal homepage: http://MACS.journals.semnan.ac.ir

Theoretical, numerical, and experimental analyses of free vibrations of glass fiber reinforced polymer plates with central cutouts and free boundaries

S. Soleimanian, A. Davar*, R. Azarafza, J.E. Jam, M.R. Zamani

University Complex of Materials and Manufacturing Technology, Malek Ashtar University of Technology, Lavizan, Tehran, (98)(21)2293-2256, Iran

PAPER INFO

Paper history:
Received 2017-08-06
Revised 2017-11-25
Accepted 2018-01-02

Keywords:
Free vibration
GFRP plates
Cutout
Free boundaries

ABSTRACT

This study explored the free vibration problem in relation to glass fiber reinforced polymer (GFRP) plates with central cutouts and free boundaries using theoretical, experimental, and numerical methods. The theoretical formulations were derived from the classical lamination plate theory. The rectangular cutout was mathematically modeled into the stiffness matrix of the plate by multiplying Heaviside distribution functions. The theoretical values for the fundamental frequency were obtained by solving the standard eigenvalue problem, and the theoretical solution was validated by comparison to the literature. Modal testing was performed in the laboratory. For additional validation, the accuracy of theoretical and experimental results was checked using the finite element method and ABAQUS. The results of all three methods agreed; thus, the applicability of the Heaviside functions to stiffness modeling of structures with cutouts was proven. It was also observed that the fundamental frequency decreased when cutout size increased.

1. Introduction

The free vibration problem related to composite plates has been extensively studied using theoretical, numerical, and experimental methods. Cutouts can be made in glass fiber reinforced polymer (GFRP) plates for practical purposes, such as decreasing structural weight and improving buckling behavior. To define cutout regions mathematically, some researchers have used mapping functions, while others have utilized thickness distribution or stiffness distribution functions.

Leissa [1] proposed closed form expressions for vibration frequencies of rectangular plates with various boundary conditions based on beam functions using the Ritz method. Singal et al. [2] carried out experimental analyses to evaluate the resonant frequency values of isotropic plates with free boundaries. Wang [3] analysed free vibrations of angle-ply symmetric laminated plates with free boundaries using discrete singular convolution, which provided accurate results for high modes of frequency. Reddy [4] developed a shear deformable theory using the finite element method (FEM) to analyze the vibrations of layered composites with cutouts. Paramasivam [5] developed finite difference operators to study the effect of openings on the fundamental frequency of plates by considering different types of boundary conditions. Yettram and Brown [6] studied the elastic stability of square perforated plates with simply supported boundaries, subjected to bi-axial loading using a finite difference method. Choi et al. [7] proposed a finite element analysis for perforated plates with free boundaries by introducing cosine shape func-

* Corresponding author.
E-mail address: davar78@gmail.com, a_davar@mut.ac.ir

DOI: 10.22075/MACS.2018.12167.1116

tions. Talabatake et al. [8] presented material modeling using the unit step function to define structure stiffness based on Galerkin's method to solve the differential equation of equilibrium. Rezaeepazhand and Jafari [9] presented a theoretical solution for stress analysis of composite plates with various central cutout shapes using a general mapping function, stating its ability to change stress concentrations in perforated plates significantly. Azhari et al. [10] studied the buckling problem in stepped and perforated plates by defining subregions with different thicknesses using interpolation functions. Li and Cheng [11] presented Heaviside distribution functions to model the stiffness of orthogrid sandwich panels locally; due to the difficulty of improving local material modeling, the solution was simplified to consider only symmetric sandwich layups. Lee [12] studied the dynamic stability of laminated composite skew plates with or without cutouts using the FEM. Erklig et al. [13] studied the effect of cutouts on the natural frequency of composite plates using the FEM and experimental analyses. Chen et al. [14] presented a unique work that provided the energy functional of a plate with a cutout by integrating the plate domain to study the plate flexural and in-plane vibrations. They showed that the location of a cutout could significantly affect structural vibration behavior. Narayana et al. [15] used the FEM to study the buckling behavior of composite plates with cutouts subjected to linearly varying in-plane loads. Kalita and Haldar used the same method to study the static [16] and free vibration [17] problems related to isotropic and orthotropic plates with central cutouts. Joshi et al. [18] examined the stress concentration factor for isotropic and orthotropic plates with central cutouts using the FEM and showed that plates with square cutouts had higher stress concentrations than those with triangular cutouts. Rajana et al. [19] studied the effect of boundary conditions on the buckling characteristics of laminated composite plates with and without cutouts using the FEM and observed that the panel with a larger cutout offers had higher buckling resistance compared to the panel without a cutout. Dharshani [20] investigated the deflection and failure of GFRP stiffened composite plates with rectangular cutouts subjected to axial and lateral loading using a finite element analyses and experiments.

In this study, a GFRP plate with a central cutout was modeled using a mathematical method. In comparison to numerical methods, mathematical tools can run analyses in less time and can be improved to obtain more accurate results for future plate theory research. Here, Heaviside distribution functions were used to define local stiffness tensor, and an analytical solution to the free vibration problem was presented using the closed form Galerkin's method. Galerkin method integrations are solved by symbolic computation using MATLAB. The main innovation of this analytical approach to the free vibration problem is that it considers free boundaries. A finite element model of the problem was made based on S4R elements using ABAQUS. To perform modal experiments, a GFRP plate was fabricated by hand layup, with a central cutout created by machining the plate. A system of linked devices for modal testing was created to measure the fundamental frequency of the plate. Finally, the theoretical, ABAQUS, and experimental results for different sized cutouts were compared. The general mathematical model, which can be used to analyze symmetric and asymmetric laminates with central cutouts, is the innovative result of the present work. Another novel contribution is the free boundary conditions applied at all edges of the structure.

2. Analyses

2.1 Theoretical approach

A plate with a rectangular cutout was placed at $(0,0,0) \leq (x,y,z) \leq (a,b,h)$ (Figure 1).

To define the cutout position, Heaviside distribution functions were introduced using Eqs. 1(a) and 1(b) [11],

$$H(x) = Heaviside\left(x - x_c + {}^{c}\!/_{2}\right) - Heaviside\left(x - x_c - {}^{c}\!/_{2}\right) \quad (1a)$$

and

$$H(y) = Heaviside\left(y - y_c + {}^{d}\!/_{2}\right) - Heaviside\left(y - y_c - {}^{d}\!/_{2}\right) \quad (1b)$$

where (x_c, y_c) is the center of the cutout. The parameters c and d are the length and width of the cutout. The Heaviside distribution (HD) function is given by Eq. (2) [11].

$$HD = 1 - H(x).H(y) \quad (2)$$

In Figure 2, values of one and zero are allocated to white and black regions.

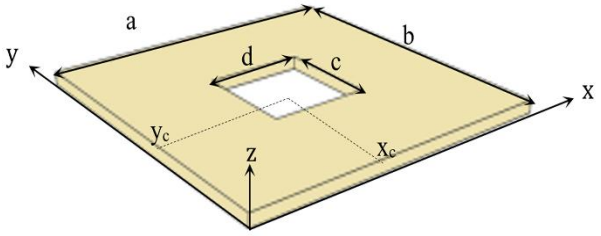

Figure 1. Plate with rectangular cutout

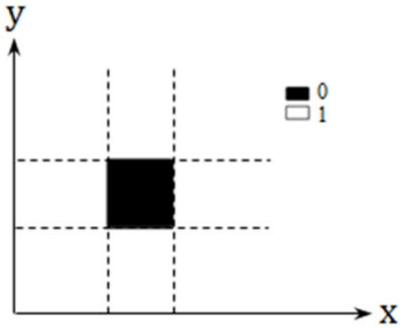

Figure 2. Plot of the *HD* function

The stiffness matrix of a lamina with a central cutout can be given as

$$Q(x,y)^k = Q^k.HD \tag{3}$$

where Q^k is the stiffness matrix of an orthotropic lamina given by Eq. 4 [6],

$$Q^k = \begin{bmatrix} \frac{E_1}{1-\upsilon_{12}\upsilon_{21}} & \frac{\upsilon_{12}E_2}{1-\upsilon_{12}\upsilon_{21}} & 0 \\ \frac{\upsilon_{21}E_1}{1-\upsilon_{12}\upsilon_{21}} & \frac{E_2}{1-\upsilon_{21}\upsilon_{12}} & 0 \\ 0 & 0 & G_{12} \end{bmatrix} \tag{4}$$

Here, E_1, E_2, $\upsilon_{ij,}$ and G_{12} are longitudinal the elastic modulus, transverse elastic modulus, Poisson's ratio, and shear modulus, respectively. The linear displacement field is given as in [6].

$$u(x,y,z) = u_0(x,y,z) - zw_{0,x}(x,y) \tag{5}$$

$$v(x,y,z) = v_0(x,y,z) - zw_{0,y}(x,y) \tag{6}$$

$$w(x,y,z) = w_0(x,y) \tag{7}$$

Using classical lamination plate theory, equilibrium equations were derived as in [6].

$$N_{x,x} + N_{xy,y} = \rho h\ddot{u}_0 \tag{8}$$

$$N_{xy,x} + N_{y,y} = \rho h\ddot{v}_0 \tag{9}$$

$$M_{x,xx} + 2M_{xy,xy} + M_{y,yy} = \rho h\ddot{w}_0 \tag{10}$$

Force and moment results are given by [6].

$$\begin{bmatrix} N_x \\ N_y \\ N_{xy} \\ M_x \\ M_y \\ M_{xy} \end{bmatrix} = \begin{bmatrix} A_{11} & A_{12} & A_{16} & B_{11} & B_{12} & B_{16} \\ A_{21} & A_{22} & A_{26} & B_{21} & B_{22} & B_{26} \\ A_{61} & A_{62} & A_{66} & B_{61} & B_{62} & B_{66} \\ B_{11} & B_{12} & B_{16} & D_{11} & D_{12} & D_{16} \\ B_{21} & B_{22} & B_{26} & D_{21} & D_{22} & D_{26} \\ B_{61} & B_{62} & B_{66} & D_{61} & D_{62} & D_{66} \end{bmatrix} \begin{bmatrix} u_{0,x} \\ v_{0,y} \\ u_{0,y} + v_{0,x} \\ -w_{0,xx} \\ -w_{0,yy} \\ -2w_{0,xy} \end{bmatrix} \tag{11}$$

Here, A, B, and D coefficients can be obtained by [6].

$$A_{ij} = \sum_{k=1}^{N} \left(Q_{ij}\right)_k \left(z_k - z_{k-1}\right) \tag{12}$$

$$B_{ij} = \frac{1}{2}\sum_{k=1}^{N} \left(Q_{ij}\right)_k \left({z_k}^2 - {z_{k-1}}^2\right) \tag{13}$$

$$D_{ij} = \frac{1}{3}\sum_{k=1}^{N} \left(Q_{ij}\right)_k \left({z_k}^3 - {z_{k-1}}^3\right) \tag{14}$$

The governing equilibrium equations can be obtained by substituting Eq. (11) with Eqs. (8-10) as:

$$\begin{aligned} &\left(A_{11,x} + A_{16,y}\right)u_{0,x} + \left(A_{16,x} + A_{66,y}\right)u_{0,y} + \\ &\left(A_{16,x} + A_{66,y}\right)v_{0,x} + \left(A_{12,x} + A_{26,y}\right)v_{0,y} - \\ &\left(B_{11,x} + B_{16,y}\right)w_{0,xx} - 2\left(B_{16,x} + B_{66,y}\right)w_{0,xy} - \\ &\left(B_{12,x} + B_{26,y}\right)w_{0,yy} + A_{11}u_{0,xx} + 2A_{16}u_{0,xy} + \\ &A_{66}u_{0,yy} + A_{16}v_{0,xx} + \left(A_{12} + A_{66}\right)v_{0,xy} + \\ &A_{26}v_{0,yy} - B_{11}w_{0,xxx} - 3B_{16}w_{0,xxy} - \\ &\left(B_{12} + 2B_{66}\right)w_{0,xyy} - B_{26}w_{0,yyy} + \\ &N_x^i u_{xx} + N_y^i u_{yy} + N_{xy}^i u_{xy} = \rho h\ddot{u}_0 \end{aligned} \tag{15}$$

$$\begin{aligned} &\left(A_{16,x} + A_{12,y}\right)u_{0,x} - \left(A_{66,x} + A_{26,y}\right)u_{0,y} + \\ &\left(A_{66,x} + A_{26,y}\right)v_{0,x} + \left(A_{26,x} + A_{22,y}\right)v_{0,y} - \\ &\left(B_{16,x} + B_{12,y}\right)w_{0,xx} - 2\left(B_{66,x} + B_{26,y}\right)w_{0,xy} - \\ &\left(B_{26,x} + B_{22,y}\right)w_{0,yy} + A_{16}u_{0,xx} + \\ &\left(A_{12} + A_{66}\right)u_{0,xy} + A_{26}u_{0,yy} + A_{66}v_{0,xx} + \\ &2A_{26}v_{0,xy} + A_{22}v_{0,yy} - B_{16}w_{0,xxx} - \\ &\left(B_{12} + 2B_{66}\right)w_{0,xxy} - 3B_{26}w_{0,xyy} - \\ &B_{22}w_{0,yyy} + N_x^i v_{xx} + N_y^i v_{yy} + N_{xy}^i v_{xy} = \rho h\ddot{v}_0 \end{aligned} \tag{16}$$

$$\begin{aligned} &\left(B_{11,xx} + 2B_{16,xy} + B_{12,yy}\right)u_{0,x} + \\ &\left(B_{16,xx} + 2B_{66,xy} + B_{26,yy}\right)u_{0,y} + \\ &\left(B_{16,xx} + 2B_{66,xy} + B_{26,yy}\right)v_{0,x} + \\ &\left(B_{12,xx} + 2B_{26,xy} + B_{22yy}\right)v_{0,y} - \\ &\left(D_{11,xx} + 2D_{16,xy} + D_{12,yy}\right)w_{0,xx} - \\ &\left(2D_{16,xx} + 4D_{66,xy} + 2D_{26,yy}\right)w_{0,xy} - \\ &\left(D_{12,xx} + 2D_{26,xy} + D_{22,yy}\right)w_{0,yy} + \\ &2\left(B_{11,x} + B_{16,y}\right)u_{0,xx} + 2\left(2B_{16,x} + B_{66,y} + B_{12,y}\right) \\ &u_{0,xy} + 2\left(B_{66,x} + B_{26,y}\right)u_{0,yy} + \\ &2\left(B_{16,x} + B_{66,y}\right)v_{0,xx} + 2\left(B_{12,x} + 2B_{26,y} + B_{66,x}\right) \\ &v_{0,xy} + 2\left(B_{26,x} + B_{22,y}\right)v_{0,yy} - \\ &2\left(D_{11,x} + D_{16,y}\right)w_{0,xxx} - \\ &\left(6D_{16x} + 2D_{12,y} + 4D_{66,y}\right)w_{0,xxy} - \\ &\left(2D_{12,x} + 6D_{26,y} + 4D_{66,x}\right)w_{0,xxy} - \\ &2\left(D_{22,y} + D_{26,x}\right)w_{0,yyy} + B_{11}u_{0,xxx} + \\ &3B_{16}u_{0,xxy} + \left(2B_{66} + B_{12}\right)u_{0,xyy} + \\ &B_{26}u_{0,yyy} + B_{16}v_{0,xxx} + \left(B_{12} + 2B_{66}\right)v_{0,xxy} + \\ &3B_{26}v_{0,xyy} + B_{22}v_{0,yyy} - D_{11}w_{0,xxxx} - 4D_{16}w_{0,xxxy} - \\ &\left(2D_{12} + 4D_{66}\right)w_{0,xxyy} - 4D_{26}w_{0,xyyy} - \\ &D_{22}w_{0,yyyy} + N_x^i w_{xx} + N_y^i w_{yy} + N_{xy}^i w_{xy} = \rho h\ddot{w}_0 \end{aligned} \tag{17}$$

Here, the second indices are devoted to local derivatives. Considering displacement shape functions corresponding to free edge conditions as in [18],

$$u_0(x,y) = U_{mn}\cos\left(\frac{m\pi}{a}x\right)\cos\left(\frac{n\pi}{b}y\right) \tag{18}$$

$$v_0(x,y) = V_{mn}\cos\left(\frac{m\pi}{a}x\right)\cos\left(\frac{n\pi}{b}y\right) \tag{19}$$

$$w_0(x,y) = W_{mn}\cos\left(\frac{m\pi}{a}x\right)\cos\left(\frac{n\pi}{b}y\right) \tag{20}$$

and using the Galerkin method, the system of partial differential equations given by Eqs. (15–17) lead to Eq. (21),

$$[M]\{\ddot{\delta}\}+[K]\{\delta\}=0 \quad (21)$$

where K and M refer to stiffness and the mass matrix coefficient, respectively. M is the mass matrix and δ is the displacement vector. K and M matrices are expanded in appendices A and B, which have been obtained through MATLAB symbolic computations. The fundamental frequency can be obtained as

$$([K]-\omega^2[M])\delta=0 \quad (22)$$

where ω is the Eigen frequency. By applying the MATLAB *Eigen* command, the frequency value can be achieved.

2.2 FEM approach

The FEM was used for the present problem and applied in ABAQUS. The structure was combined with S4R elements, and the FEM meshed model (Figure 3) was produced using S4R elements. Performing a numerical modal analysis using the Lanczos eigensolver, the fundamental structural frequency can be obtained in ABAQUS.

2.3 Experimental approach

2.3.1 Fabrication process

The fabrication process is carried out in a workshop at 22°C and 33% humidity. A GFRP plate with a $[0/90]_5$ layup was fabricated using a hand-layup. A cold-cure epoxy system was provided with a 100:55 mixing ratio, and to reinforce the plate, a unidirectional (UD) e-glass fiber (Figure 4) was used. Using a matrix-impregnated spatula, the UD fiber layer was completely covered by the epoxy matrix (Figure 5) and further impregnation of fibers was provided by a brush.

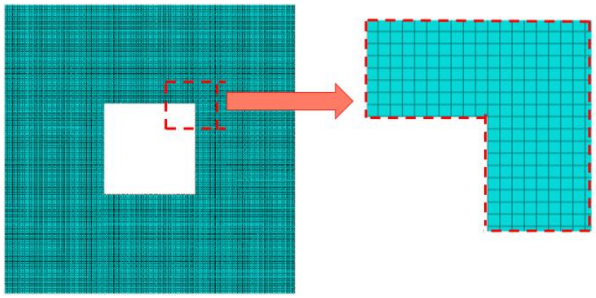

Figure 3. Meshed FEM

Figure 4. Epoxy impregnated UD e-glass fiber

The GFRP plate was left to cure at room temperature for 48 hours, and the final product was machined to obtain an acceptable edge smoothness and accurate dimensions (Figure 5). The GFRP plate length was 0.35 m. The central cutout was also made during the machining process.

2.3.2 Burn test

To measure the volume fraction of the fiber and matrix, six composite specimens were burned in a furnace at 550°C for one hour (Figure 6). Figures 7a and 7b show the composite specimens before and after the burn test, respectively.

Figure 5. Machining of the GFRP plate

Figure 6. Putting the GFRP specimens in the furnace

(a)

(b)

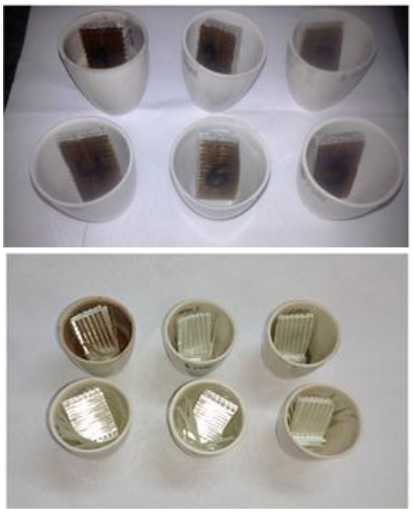

Figure 7. GFRP samples: (a) before burning; (b) after burning

Based on the burn test, the volume fraction of the fibers was 45.77%. By applying micromechanical rules to the pure glass fiber and resin material properties, the GFRP lamina properties were calculated (Table 1).

2.3.2 Experimental modal test

The experimental modal test was carried out following a single-input, single-output scheme using a hammer, acceleration sensor, analyzer, and data collector linked together. To provide the proper free edge conditions, the GFRP plate was hung from the ceiling using a narrow band (Figure 8).

3. Results

3.1 Verification of the theoretical solution

As shown in Table 2, the accuracy of the present theoretical solution was examined using the results obtained by Leissa [1] relating to free vibration of rectangular plates with free boundaries, and the results agreed.

Table 1. Mechanical and physical properties of the GFRP lamina

E_{11} [GPa]	E_{22} [GPa]	G_{12} [GPa]	υ_{12}	ρ [kg/m³]
40.745	10.395	3.242	0.254	1658.357

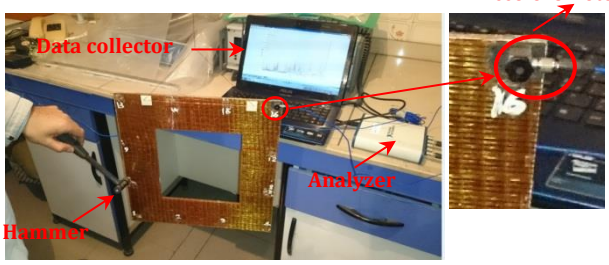

Figure 8. Modal experiment setup, including the freely suspended plate and the test devices

Table 2. Comparison study results for non-dimensional frequency parameter $\omega a^2\sqrt{12\rho(1-\upsilon^2)/Eh^3}$

a [mm]	b [mm]	Theoretical	Leissa (1992)	Discrepancy (%)
25.4	25.4	82.538	81.84	0.85
25.4	38.1	55.026	54.21	1.5

3.2 Parametric study of the size of the central cutout

Parametric studies were carried out to determine variations in the fundamental frequency the plates by changing the cutout size. The volume fraction of the central cutout is defined as

$$R = m_x n_y \frac{c \times d}{a \times b} \times 100 \qquad (23)$$

Considering R = 0, 10%, and 20%, the present study results are reported in Figures 9, 10, and 11, respectively. All theoretical, experimental, and FEM results indicate that the fundamental frequency decreased as the size of the cutout increased. By increasing the cutout size, the thin plate became a square frame with a higher thickness-to-side length ratio near the boundaries; accordingly, the discrepancy between theoretical and ABAQUS results increased as the cutout size increased. The mode shape results showed that the free edge of the GFRP plates vibrated at the corresponding fundamental frequency in a twisting behavior.

$\omega_{Experimental}$=65 [Hz]

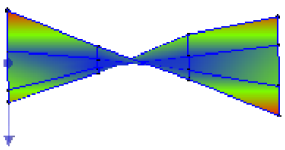

$\omega_{Theoretical}$=73.52 [Hz]

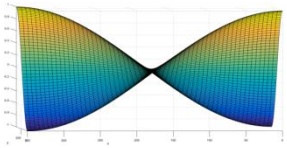

ω_{ABAQUS}=72.78 [Hz]

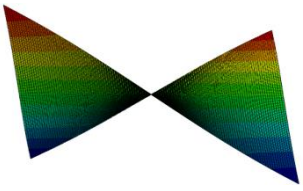

Figure 9. Fundamental frequency and mode shape (R = 0%)

$\omega_{Experimental}$=59.5 [Hz]

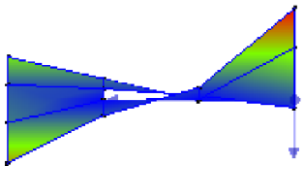

$\omega_{Theoretical}$=63.67 [Hz]

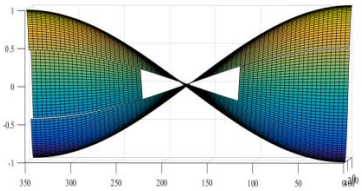

ω_{ABAQUS}=67.62 [Hz]

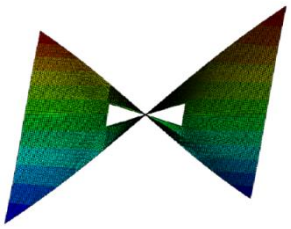

Figure 10. Fundamental frequency and mode shape (R = 10%)

$\omega_{Experimental}$=51.4 [Hz]

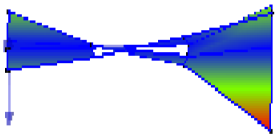

$\omega_{Theoretical}$=53.64 [Hz]

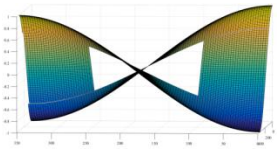

ω_{ABAQUS}=62.827 [Hz]

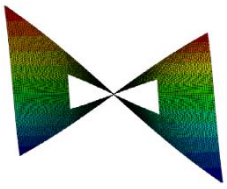

Figure 11. Fundamental frequency and mode shape (R = 20%)

The GFRP plate was fabricated by hand layup, which caused material inhomogeneity that may have affected the natural frequency and mode shape obtained in the experiment. Furthermore, the damping effect, environmental conditions, and human error were not considered when using theoretical and numerical methods, which could affect the mode shape during experiments. As a result, differences occurred when comparing theoretical and numerical mode shapes to experimental mode shapes.

4. Conclusion

Material modeling of GFRP plates with central cutouts can be successfully performed using Heaviside distribution functions. Difficulty in deriving and solving governing equations for asymmetric laminated composites with rectangular cutouts was overcome using MATLAB symbolic computations. Comparing present theoretical results and those obtained by Leissa [1], an acceptable agreement was achieved. Finally, a $[0/90]_5$ GFRP plate with a central square cutout was fabricated for experimental modal testing. By increasing the central cutout size, the results obtained using theoretical, numerical, and experimental approaches demonstrated a decreasing behaviour. The primary reason for discrepancies in the theoretical results is that increasing the ratio of c/a eliminated the efficiency of classical lamination plate theory. A major cause for errors in the experimental results was the inhomogeneous distribution of material in the GFRP plate. From these methods, the fundamental vibration mode shape for free edge GFRP plates is a twisting shape.

Appendices:

Appendix A:

$$k_{11} = \int_0^b \int_0^a \Big((A_{11,x} + A_{16,y})u_{0,x} + (A_{16,x} + A_{66,y})u_{0,y} + A_{16}u_{0,xx} + (A_{12} + A_{66})u_{0,xy} + A_{26}u_{0,yy} \Big) \cos\left(\frac{m\pi}{a}x\right) \cos\left(\frac{n\pi}{b}y\right) dxdy$$

$$k_{12} = \int_0^b \int_0^a \Big((A_{16,x} + A_{66,y})v_{0,x} + (A_{12,x} + A_{26,y})v_{0,y} + A_{16}v_{0,xx} + (A_{12} + A_{66})v_{0,xy} + A_{26}v_{0,yy} \Big) \cos\left(\frac{m\pi}{a}x\right) \cos\left(\frac{n\pi}{b}y\right) dxdy$$

$$k_{13} = \int_0^b \int_0^a \big(-(B_{11,x} + B_{16,y})w_{0,xx} - 2(B_{16,x} + B_{66,y})w_{0,xy} - (B_{12,x} + B_{26,y})w_{0,yy} - B_{11}w_{0,xxx} - 3B_{16}w_{0,xxy} - (B_{12} + 2B_{66})w_{0,xyy} - B_{26}w_{0,yyy} \big) \cos\left(\frac{m\pi}{a}x\right) \cos\left(\frac{n\pi}{b}y\right) dxdy$$

$k_{21} =$
$\int_0^b \int_0^a \int_{-h/2}^{h/2} \left((A_{16,x} + A_{12,y}) u_{0,x} - (A_{66,x} + A_{26,y}) u_{0,y} + A_{16} u_{0,xx} + (A_{12} + A_{66}) u_{0,xy} + A_{26} u_{0,yy} \right) \cos\left(\frac{m\pi}{a} x\right) \cos\left(\frac{n\pi}{b} y\right) dxdydz$

$k_{22} =$
$\int_0^b \int_0^a \left((A_{66,x} + A_{26,y}) v_{0,x} + (A_{26,x} + A_{22,y}) v_{0,y} + A_{66} v_{0,xx} + 2A_{26} v_{0,xy} + A_{22} v_{0,yy} \right) \cos\left(\frac{m\pi}{a} x\right) \cos\left(\frac{n\pi}{b} y\right) dxdy$

$k_{23} =$
$\int_0^b \int_0^a \left(-(B_{16,x} + B_{12,y}) w_{0,xx} - 2(B_{66,x} + B_{26,y}) w_{0,xy} - (B_{26,x} + B_{22,y}) w_{0,yy} - B_{16} w_{0,xxx} - (B_{12} + 2B_{66}) w_{0,xxy} - 3B_{26} w_{0,xyy} - B_{22} w_{0,yyy} \right) \cos\left(\frac{m\pi}{a} x\right) \cos\left(\frac{n\pi}{b} y\right) dxdy$

$k_{31} =$
$\int_0^b \int_0^a \left((B_{11,xx} + 2B_{16,xy} + B_{12,yy}) u_{0,x} + (B_{16,xx} + 2B_{66,xy} + B_{26,yy}) u_{0,y} + 2(B_{11,x} + B_{16,y}) u_{0,xx} + 2(2B_{16,x} + B_{66,y} + B_{12,y}) u_{0,xy} + 2(B_{66,x} + B_{26,y}) u_{0,yy} + B_{11} u_{0,xxx} + 3B_{16} u_{0,xxy} + (2B_{66} + B_{12}) u_{0,xyy} + B_{26} u_{0,yyy} \right) \cos\left(\frac{m\pi}{a} x\right) \cos\left(\frac{n\pi}{b} y\right) dxdy$

$k_{32} =$
$\int_0^b \int_0^a \int_{-h/2}^{h/2} \left((B_{16x,x} + 2B_{66,xy} + B_{26,yy}) v_{0,x} + (B_{12,xx} + B_{26,xy} + B_{22yy}) v_{0,y} + 2(B_{16,x} + B_{66,y}) v_{0,xx} + 2(B_{12,xx} + 2B_{26,y} + B_{66,x}) v_{0,xy} + 2(B_{26,x} + B_{22,y}) v_{0,yy} + B_{16} v_{0,xxx} + (B_{12} + 2B_{66}) v_{0,xxy} + 3B_{26} v_{0,xyy} + B_{22} v_{0,yyy} \right) \cos\left(\frac{m\pi}{a} x\right) \cos\left(\frac{n\pi}{b} y\right) dxdy$

$k_{33} =$
$\int_0^b \int_0^a \left(-(D_{11,xx} + 2D_{16,xy} + D_{12,yy}) w_{0,xx} - (2D_{16,xx} + 4D_{66,xy} + 2D_{26,yy}) w_{0,xy} - (D_{12,xx} + 2D_{26,xy} + D_{22,yy}) w_{0,yy} - 2(D_{11,x} + D_{16,y}) w_{0,xxx} - 2(D_{11,x} + D_{16,y}) w_{0,xxx} - (6D_{16x} + 2D_{12,y} + 4D_{66,y}) w_{0,xxy} - (2D_{12,x} + 6D_{26,y} + 4D_{66,x}) w_{0,xyy} - 2(D_{22,y} + D_{26,x}) w_{0,yyy} - D_{11} w_{0,xxxx} - (2D_{12} + 4D_{66}) w_{0,xxyy} - 4D_{26} w_{0,xyyy} - D_{22} w_{0,yyyy} \right) \cos\left(\frac{m\pi}{a} x\right) \cos\left(\frac{n\pi}{b} y\right) dxdy$

Appendix B:

$$M_{11} = \int_0^a \int_0^b \int_0^t \rho \cos\left(\frac{m\pi}{a} x\right) \cos\left(\frac{n\pi}{b} y\right) dxdy$$

$$M_{12} = 0$$

$$M_{13} = 0$$

$$M_{21} = 0$$

$$M_{22} = \int_0^a \int_0^b \int_0^t \rho \cos\left(\frac{m\pi}{a} x\right) \cos\left(\frac{n\pi}{b} y\right) dxdydz$$

$$M_{31} = 0$$

$$M_{32} = 0$$

$$M_{33} = \int_0^a \int_0^b \int_0^t \rho \cos\left(\frac{m\pi}{a} x\right) \cos\left(\frac{n\pi}{b} y\right) dxdydz$$

References

[1] Leissa AW. The free vibration of rectangular plates. *Journal of Sound and vibration* 1973; 31(3): 257-93.

[2] Singal R, Gorman D, Forgues S. A comprehensive analytical solution for free vibration of rectangular plates with classical edge coditions: Experimental verification. *Experimental Mechanics* 1992; 32(1): 21-3.

[3] Wang X. Free vibration analysis of angle-ply symmetric laminated plates with free boundary conditions by the discrete singular convolution. *Compos. Struct.* 2017; 170: 91-102.

[4] Reddy J. Large amplitude flexural vibration of layered composite plates with cutouts. *Journal of Sound and Vibration* 1982; 83(1): 1-10.

[5] Paramasivam P. Free vibration of square plates with square openings. *Journal of Sound Vibration* 1973; 30: 173-8.

[6] Yettram A, Brown C. The elastic stability of square perforated plates. *Computers & structures* 1985; 21(6): 1267-72.

[7] Choi S, Jeong K, Kim T, Kim K, Park K. Free vibration analysis of perforated plates using equivalent elastic properties. *Nuclear Engineering and Technology* 1998; 30(5): 416-23.

[8] Hideo T. Static analyses of elastic plates with voids. *International Journal of Solids and Structures* 1991; 28(2): 179-96.

[9] Rezaeepazhand J, Jafari M. Stress analysis of perforated composite plates. *Compos. Struct.* 2005; 71(3-4): 463-8.

[10] Azhari M, Shahidi A, Saadatpour M. Local and post local buckling of stepped and perforated thin plates. *Applied Mathematical Modelling* 2005; 29(7): 633-52.

[11] Li G, Cheng J. A generalized analytical modeling of grid stiffened composite structures. *J. Compos. Mater.* 2007; 41(24): 2939-69.
[12] Lee S-Y. Finite element dynamic stability analysis of laminated composite skew plates containing cutouts based on HSDT. *Compos. Sci. Technol.* 2010; 70(8): 1249-57.
[13] Erkliğ A, Bulut M, Yeter E. Effects of cutouts on natural frequency of laminated composite plates. *Science and Engineering of Composite Materials* 2013; 20(2): 179-85.
[14] Chen Y, Jin G, Liu Z. Flexural and in-plane vibration analysis of elastically restrained thin rectangular plate with cutout using Chebyshev–Lagrangian method. *International Journal of Mechanical Sciences* 2014; 89: 264-78.
[15] Narayana AL, Rao K, Kumar RV. Buckling analysis of rectangular composite plates with rectangular cutout subjected to linearly varying in-plane loading using fem. *Sadhana* 2014; 39(3): 583-96.
[16] Kalita K, Halder S. Static analysis of transversely loaded isotropic and orthotropic plates with central cutout. *Journal of the Institution of Engineers (India): Series C* 2014; 95(4): 347-58.
[17] Kalita K, Haldar S. Free vibration analysis of rectangular plates with central cutout. *Cogent Engineering* 2016; 3(1): 1163781.
[18] Joshi S, Jadvani N, Shinde D, Kalita K. SCF in Isotopic & Orthotropic Plates Part II: Biaxial Load. *Materials Today: Proceedings* 2017; 4(2): 2639-44.
[19] Rajanna T, Banerjee S, Desai YM, Prabhakara D. Effect of boundary conditions and non-uniform edge loads on buckling characteristics of laminated composite panels with and without cutout. *International Journal for Computational Methods in Engineering Science and Mechanics* 2017; 18(1): 64-76.
[20] Priyadharshani SA, Prasad AM, Sundaravadivelu R. Analysis of GFRP stiffened composite plates with rectangular cutout. *Compos. Struct.* 2017; 169: 42-51.